Note: Femtosecond laser micromachining of straight and linearly tapered capillary discharge waveguides

S. M. Wiggins,[a] M. P. Reijnders,[b] S. Abuazoum, K. Hart, G. H. Welsh, R. C. Issac, D. R. Jones, and D. A. Jaroszynski
Scottish Universities Physics Alliance, Department of Physics, University of Strathclyde, Glasgow G4 0NG, United Kingdom

Gas-filled capillary discharge waveguides are important structures in laser-plasma interaction applications, such as the laser wakefield accelerator. We present the methodology for applying femtosecond laser micromachining in the production of capillary channels (typically 200–300 μm in diameter and 30–40 mm in length), including the formalism for capillaries with a linearly tapered diameter. The latter is demonstrated to possess a smooth variation in diameter along the length of the capillary (tunable with the micromachining trajectories). This would lead to a longitudinal plasma density gradient in the waveguide that may dramatically improve the laser-plasma interaction efficiency in applications. © *2011 American Institute of Physics*. [doi:10.1063/1.3640410]

Femtosecond laser micromachining (FLM) is a valuable tool in scientific and industrial applications because, at high intensity ($\sim10^{15}$ W/cm^2), multiphoton absorption and avalanche ionization processes allow high precision, small scale laser ablation to be carried out in even the hardest dielectric materials.[1] It is superior to mechanical micromilling techniques since the ablation size scale is of the order of the laser focal spot size (~10 μm) and it outperforms nanosecond laser micromachining because the laser pulse duration is much shorter than the time scale for thermal diffusion (typically ns). FLM is precise, repeatable, and deterministic,[2] thus making it an ideal method for the production of capillary channels[3] utilized as gas-filled capillary discharge waveguides (CDWs).[4,5]

CDWs are advantageous in high-intensity (up to $\sim10^{19}$ W/cm^2 to date) laser-plasma applications, such as the laser wakefield accelerator[6] and Raman amplifier,[7] because laser pulses can be successfully guided over several centimetres, thereby extending the interaction length (much longer than the Rayleigh length).[4] Plasma is formed in a gas-filled CDW before the laser pulse arrival time by injection of gas (usually hydrogen) and subsequent ionization by a ~20 kV, ~1 μs electrical discharge pulse. Recently, we developed a new power supply unit based on high-voltage solid-state switching and wound transmission line transformer technology to reliably deliver such pulses.[8]

Hard materials such as alumina or sapphire are employed for the waveguides to maximize robustness in view of the high voltages and high laser intensities they are subjected to. As a consequence, FLM has become a common technique for their production.[3] Here, we outline this technique for uniform, straight capillaries and then extend it by describing the micromachining trajectories needed to produce a linearly tapered capillary diameter. Tapering the diameter, i.e., the cross section, leads to a taper in the longitudinal plasma density.[9] In laser wakefield accelerator applications, theoretical studies[10,11] have predicted a substantial increase in electron beam energy upon laser pulse propagation through a positively tapered plasma density gradient (lower to higher density). It may also increase the seed laser pulse amplification efficiency in the chirped pulse Raman amplifier.[12] Formation of a smoothly tapered capillary is demonstrated with optical microscopy images of the finished surface.

To create the waveguide, laser ablation is performed on two dielectric plates such that each has a longitudinal hemispherical groove machined out along their length. A circular cross-section capillary channel is then formed by aligning and gluing the two plates together. One of the plates has additional surface grooves or bore holes micromachined into it to allow for gas injection into the capillary. The surface groove method requires careful plate alignment to enable a good O-ring seal around the gas fittings; therefore, our preference is for the bore hole method (hole dimensions $\sim700 \times 200$ μm, located 5 mm from the ends). Positioned at either end of the capillary are copper electrodes (with on-axis apertures enable the laser pulses to propagate) coupled to the output of a high voltage pulsed power supply. Applying a potential difference of ~20 kV across the capillary (typically 30–40 mm in length) causes rapid avalanche breakdown to occur, and a high current (~300 A) discharge pulse is the evidence of near complete ionization of the gas in the capillary.[8]

The experimental setup to perform FLM utilizes a high repetition rate laser beam from the Strathclyde Terahertz to Optical Pulse Source (TOPS) Ti:sapphire femtosecond laser system[13] (Gaussian profile, average power up to 500 mW, duration 50 fs and 1 kHz pulse repetition rate) that is focused by a 60 mm focal length lens to a waist (radius at $1/e^2$) of 12 μm at the surface of the dielectric plates. The plates are mounted together on XY translation stages driven by a computer-controlled motion controller (Newport, XPS). Position and velocity commands sent to the controller determine the pattern to be machined. The plates should be sized to within ~10 μm of each other with respect to their width

---

a)Electronic mail: mark.wiggins@strath.ac.uk.
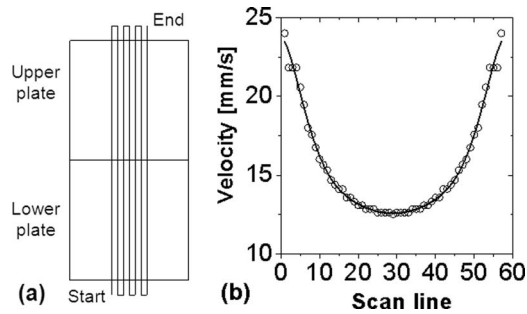b)Present address: TMC Physics, Flight Forum 107, 5657 DC Eindhoven, The Netherlands.

FIG. 1. (a) Scanning laser schematic and (b) velocity profile over $N = 57$ scan lines for machining straight CDWs where the solid line is a best-fit quadratic. The diameter $d = (N - 1) \delta x$, for example, $d = 280$ μm when $\delta x = 5$ μm.

and length and aligned to within <1 mrad of the longitudinal translation stage axis in order to facilitate acceptable alignment after machining.

Obtaining a hemispherical groove is predicated on two aspects of the FLM process. First, as a Gaussian-profile laser beam scans across the target surface, the depth profile of the ablated region is also Gaussian shaped[14] and the cross-sectional area of ablated material is inversely proportional to the scanning velocity. For the velocity range applied, the single pulses overlap such that the laser can be assumed to be continuous. Second, the laser focal waist is much less than the capillary diameter. Hence, a complete capillary comprises a series of many *longitudinal* scans (57 in our case, each repeated 16 times) at different *radial* positions [Fig. 1(a)], where close to the axis, the scan velocity is low and at the outer edges, the scan velocity is high. As shown in Fig. 1(b), a near-hemispherical scanning velocity profile is used to map into a hemispherical machined depth profile (the edges are splayed to prevent any possible fracture). The basis for machining a uniform, straight capillary is, therefore, constant velocity motion of the scanning laser along the longitudinal direction utilizing this velocity-to-depth mapping. An additional free parameter is the laser energy. An optimal energy

setting results in the desired hemispherical profile; otherwise, grooves are too shallow or too deep. The capillary diameter d is set by the radial step size δx between longitudinal scans with matched laser energy to achieve the corresponding depth profile ($d/2$ in the center).

Optical microscope images of an example straight capillary are shown in Fig. 2. The alumina capillary is of length 40 mm and nominal design diameter 280 μm. The laser pulse energy was (150 ± 10) μJ (corresponding to intensity 10^{14} W/cm^2) and the machining time is 95 min. The measured depth and widths, at either end of the capillary, are within ~ 5 μm of the desired value (280 μm ignoring the splayed edges) demonstrating a high degree of circularity to the capillary channel. Laser energy fluctuations during the reasonably long duration of machining are the primary cause of deviations from the final desired depth. Our control program (National Instruments, LABVIEW (Ref. 15)) acts to pause the machining process, if the average laser energy (monitored with a photodiode) drifts outside an acceptable range. The linear scaling of machined depth with average laser energy will determine what energy fluctuations are acceptable for a given application. In our experience, energy fluctuations of $\pm 10\%$ are tolerable in the production of CDWs.

A linear taper in the diameter requires two modifications to the machining process. First, the scanning direction is not wholly longitudinal; a small radial velocity component is also needed, clearly, to obtain the conical shape. Second, as the scanning laser progresses from the wide end to the narrow end, its velocity must increase to maintain the hemispherical ablation depth (which is inversely proportional to the velocity). Hence, the scanning laser is now accelerating instead of moving at constant velocity.

To determine the tapered capillary trajectory equations describing the evolution of the scanning laser position $x(t)$, velocity $v(t)$, and acceleration $a(t)$ as a function of time t, per scan line, consider the profile of a linearly tapered channel described by $r(x) = r_1 + \alpha x$ with the number of scan lines N constant over its length. The removed area of a cross section of one single scan line $A_{scanline} \propto 1/|v|$, so $A_{total}(x)v(x) \sim r(x)^2 v(x)$ is constant, that is $r_1^2 v(0) = r(x)^2 v(x)$, where $v(0)$ is the initial velocity for that particular scan line. Hence, the ratio between the start and end velocities is simply the square of the ratio of the radii given by $v(L)/v(0) = (r_1/r_2)^2$, where r_1 and r_2 are the start and end radii, respectively and L is the length. In general, this results in $v(x)$ being defined as $v(x) = r_1^2 v(0)/(r_1 + \alpha x)^2$, where $\alpha = (r_2 - r_1)/L$ describes the rate of tapering. With separation of variables and solving for $x_0 = 0$, this results in the trajectory equations given by

$$x(t) = \frac{1}{\alpha} \left(\sqrt[3]{3t r_1^2 v(0)\alpha + r_1^3} - r_1 \right), \quad (1)$$

$$v(t) = \frac{r_1^2 v(0)}{\left[r_1^2 3t v(0)\alpha + r_1^3 \right]^{2/3}}, \quad (2)$$

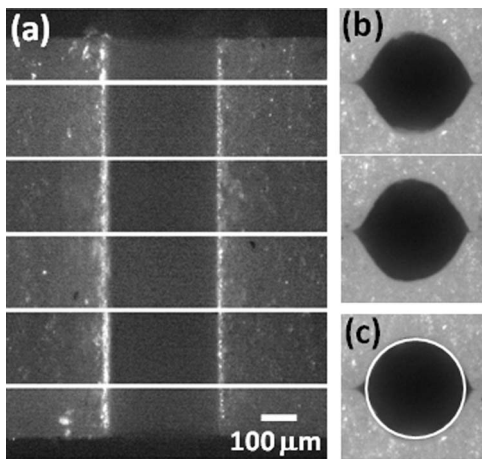$$a(t) = \frac{-2 r_1^4 v(0)^2 \alpha}{-r_1^2 [-3t v(0)\alpha - r_1]^{5/3}}. \quad (3)$$

FIG. 2. Optical microscope images of a straight CDW showing (a) sampled longitudinal positions along one plate and (b) both ends of the aligned capillary. (c) One end with a superimposed circle of diameter 280 μm. The indicated scale applies to all images.
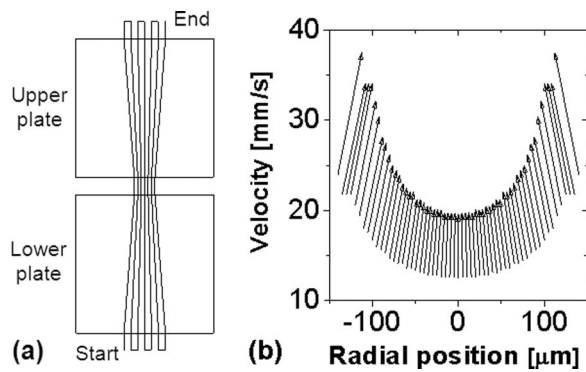
FIG. 3. (a) Scanning laser schematic for machining linearly tapered CDWs and (b) the start-to-end velocities of each scan line implemented for a diameter taper of 280 μm $\rightarrow$ 224 μm over 40 mm.

The modified scanning schematic and an example velocity profile configuration are shown in Fig. 3. Implementation is achieved using the position, velocity, and time (PVT) trajectory mode of the motion controller. There is a discrepancy of less than 1% between the ideal velocity evolution given by Eq. (2) and the real velocity evolution outcome (subject to the constraints of the PVT mode algorithm which proscribes a constant rate of change of acceleration, i.e., constant jerk, onto the motion).

Optical microscope images of an example linearly tapered capillary are shown in Fig. 4. The alumina capillary is of length 40 mm and the nominal design diameter is 280 μm $\rightarrow$ 224 μm ($\alpha = 5 \times 10^{-4}$ and laser pulse energy is ~150 μJ). Samples of the longitudinal capillary widths [Figs. 4(a) and 4(b)] demonstrate that a smooth taper from the wide end to the narrow end has been accomplished along both plates. The end-on images [Figs. 4(c) and 4(d)], after aligning the two plates together, show near circular cross sections have been formed indicating that, once again, the average laser energy was very close to the optimal (machining time in this case is 106 min). Dimensions of the major and minor axes for each best-fit ellipse are 285 $\times$ 278 μm and 234 $\times$ 233 μm,

respectively. The cross-sectional area reduction factor is, therefore, 1.45, which is a deviation of only 7% from the design value of 1.56.

In conclusion, CDWs can be effectively produced using the FLM technique and we have shown that a linear taper in the capillary cross section can be successfully implemented with appropriate acceleration of the scanning laser during the machining process. The controllability of FLM means that the final waveguide parameters can be readily tuned to suit the application conditions, for example, the degree of longitudinal plasma density tapering required for enhanced electron beam energy gain in a laser wakefield accelerator is determined by α, the rate of the cross-section taper. Producing a nonlinear taper in the cross section, as deemed highly desirable for laser wakefield accelerator application,[10,11,16] may also be possible with the micromachining technique. This would require additional acceleration in the radial direction along each scan line, matched to the appropriate longitudinal acceleration.
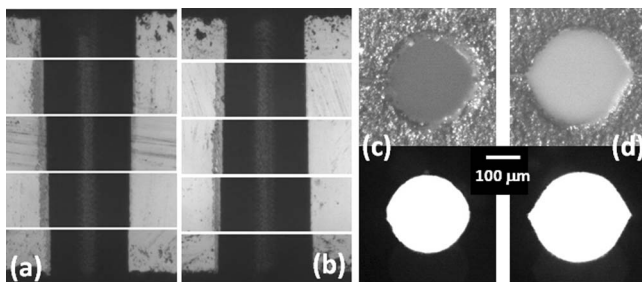
FIG. 4. Optical microscopy images of a linearly tapered CDW showing regular longitudinal positions along the (a) upper and (b) lower plate surfaces. (c) and (d) Each end of the aligned capillary, both in reflection mode and transmission mode of the microscope. The indicated scale applies to all images.

[1]R. R. Gattass and E. Mazur, Nature Photon. **2**, 219 (2008).
[2]B. C. Stuart, M. D. Feit, S. Herman, A. M. Rubenchik, B. W. Shore, and M. D. Perry, Phys. Rev. B **53**, 1749 (1996).
[3]D. A. Jaroszynski, R. Bingham, E. Brunetti, B. Ersfeld, J. Gallacher, B. van der Geer, R. Issac, S. P. Jamison, D. Jones, M. de Loos, A. Lyachev, V. Pavlov, A. Reitsma, Y. Saveliev, G. Vieux, and S. M. Wiggins, Philos. Trans. R. Soc. London, Ser. A **364**, 689 (2006).
[4]D. J. Spence and S. M. Hooker, Phys. Rev. E **63**, 015401 (2001).
[5]N. A. Brobova, A. A. Esaulov, J.-I. Sakai, P. V. Sasorov, D. J. Spence, A. Butler, S. M. Hooker, and S. V. Bulanov, Phys. Rev. E **65**, 016407 (2001).
[6]E. Esarey, C. B. Schroeder, and W. P. Leemans, Rev. Mod. Phys. **81**, 1229 (2009).
[7]V. M. Malkin, G. Shvets, and N. J. Fisch, Phys. Rev. Lett. **82**, 4448 (1999).
[8]S. Abuazoum, S. M. Wiggins, R. C. Issac, G. H. Welsh, G. Vieux, M. Ganciu, and D. A. Jaroszynski, Rev. Sci. Instrum. **82**, 063505 (2011).
[9]D. Kaganovich, P. Sasorov, C. Cohen, and A. Zigler, Appl. Phys. Lett. **75**, 772 (1999).
[10]P. Sprangle, J. R. Penano, B. Hafizi, R. F. Hubbard, A. Ting, D. F. Gordon, A. Zigler, and T. M. Antonsen, Jr., Phys. Plasmas **9**, 2364 (2002).
[11]W. Rittershofer, C. B. Schroeder, E. Esarey, F. J. Grüner, and W. P. Leemans, Phys. Plasmas **17**, 063104 (2010).
[12]G. Vieux, A. Lyachev, X. Yang, B. Ersfeld, J. P. Farmer, E. Brunetti, R. C. Issac, G. Raj, G. H. Welsh, S. M. Wiggins, and D. A. Jaroszynski, New J. Phys. **13**, 063042 (2011).
[13]D. A. Jaroszynski, B. Ersfeld, G. Giraud, S. Jamison, D. R. Jones, R. C. Issac, B. W. J. McNeil, A. D. R. Phelps, G. R. M. Robb, H. Sandison, G. Vieux, S. M. Wiggins, and K. Wynne, Nucl. Instrum. Methods Phys. Res. A **445**, 317 (2000).
[14]See, for example, A. Borowiec, M. Mackenzie, G. C. Weatherly, and H. K. Haugen, Appl. Phys. A **76**, 201 (2003).
[15]J. Travis and J. Kring, *Labview for Everyone: Graphical Programming Made Easy and Fun*, 3rd ed. (Prentice Hall, Englewood Cliffs, NJ, 2006); see http://www.ni.com/labview/ for National Instruments.
[16]T. Katsouleas, Phys. Rev. A **33**, 2056 (1986).